5

Study of Plasma Effects in HEMT-like Structures for THz Applications by Equivalent Circuit Approach

Irina Khmyrova
University of Aizu
Japan

1. Introduction

The growing interest to terahertz (THz) region of electromagnetic spectrum is pulled by a variety of its possible applications for free-space communications, sensing and imaging in radio astronomy, biomedicine, and in security screening for hidden explosives and concealed weapons. Terahertz imaging may also be useful for industrial processes, such as package inspection and quality control. Despite strong demand in compact solid-state devices capable to operate as emitters, receivers, photomixers of the THz radiation their development is still a challenging problem.

Plasma waves with linear dispersion law can exist in the gated two-dimensional electron gas (2DEG) (Chaplik 1972) in systems similar to field-effect transistor (FET) and high-electron mobility transistor (HEMT). At high enough electron mobility and gate length in submicrometer range 2DEG channel can serve as a resonant cavity for plasma waves with the resonant frequencies in the THz range. Experimentally observed infrared absorption (Allen,1977) and weak infrared emission (Tsui,1980) were related to plasma waves in silicon inversion layers. Excitation of plasma oscillations in the channel of FET-like structures has been proposed as a promising approach for the realization of emission, detection, mixing and frequency multiplication of THz radiation (Dyakonov,1993, Dyakonov,1996). Nonresonant (Weikle,1996) and weak resonant (Lu,1998) detection have been observed in HEMTs experimentally. Resonant peaks of the impedance of the capacitively contacted 2DEG at frequencies corresponding to plasma resonances have been revealed (Burke,2000). Terahertz detection and emission in HEMTs fabricated from different materials have been demonstrated (Knap,2002; Otsuji,2004; Teppe,2005; El Fatimy,2006; Shur,2003).

Theoretical models for plasma waves excited in the HEMT 2DEG channel are usually based on the similarity of the equations describing the behavior of electron fluid and shallow water (Dyakonov,1993; Shur, 2003; Satou,2003; Satou,2004; Veksler,2006). On the other hand, electromagnetic wave propagation in the gated 2DEG channel is similar to that in a transmission line (TL) (Yeager,1986; Burke,2000) which makes it possible to represent the gated portion of 2DEG channel by a TL model. In this chapter, we will implement distributed circuit or TL model approach to the study of plasma waves excited in the 2DEG channel of the structures similar to HEMT. Once a system is represented by an electric equivalent circuit, its performance can be simulated using a circuit simulator like SPICE (Simulation Program with Integrated Circuit Emphasis). Such an approach is less time consuming comparing to full scale computer modeling. It enables an easy variation of the system parameters during the simulation procedure provides a quick way to facilitate and improve one's understanding of the HEMT operation

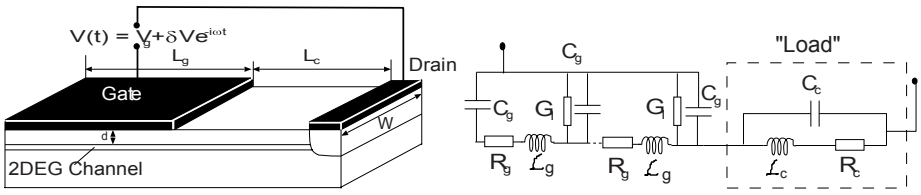

Fig. 1. Schematic structure of the HEMT (a) and its electric equivalent circuit (b). Gated portion of the 2DEG channel is represented by distributed $R\mathcal{L}C$ circuit. The rest part of the device including ungated and contact regions is enclosed in a dashed box and treated as a 'load".

in the regime of excitation of plasma wave oscillations (Khmyrova,2007). The rest of this chapter is organized as follows. In the Section 2.1 the basic electric equivalent circuit for the HEMT-like structure operating in the regime of the excitation of plasma wave oscillations is developed. Results of IsSpice simulation illustrating the dependence of resonant plasma frequency on different structure parameters are presented in Section 2.2. In the Section 2.3 load termination concept is applied to estimate reflection coefficient at the interface between gated and ungated portions of the HEMT 2DEG channel.
Section 3 focuses on the influence of the fringing effects on resonant frequency of plasma oscillations. Section 3.1 presents analytical model which allows to evaluate electric field distribution at the 2DEG surface, spatial distribution of sheet electron density, and, finally, resonant frequency of plasma oscillations in the presence of fringing effects. Section 3.2 discusses cascaded TL model and results of IsSpice simulation.
In the Section 4 results of the experiments and different analytical models are compared. Chapter summary is given in Section 5.

2. Distributed circuit approach to analysis of plasma oscillations in HEMT-like structures

2.1 Development of basic electric equivalent circuit

We consider a HEMT with schematic structure shown in Fig. 1a with a 2DEG channel formed at the heterointerface between the InGaAs narrow-gap and InAlAs wide-gap layers. Voltage $V(t) = V_g + \delta V e^{i\omega t}$ applied between the gate and drain contacts contains dc and ac components with amplitudes V_g and δV, respectively, and ac signal frequency ω. 2DEG channel beneath the gate contact of length L_g can act as a resonant cavity for the plasma waves with the fundamental resonant frequency (Dyakonov1993

$$\Omega = \frac{\pi}{2L_g}\sqrt{\frac{e^2\Sigma\, d_g}{\varepsilon_0 \varepsilon m^*}} \tag{1}$$

where e and m^* are the electron charge and effective mass, respectively, ε_0 and ε are dielectric constants of vacuum and the layer separating 2DEG channel and gate contact, thickness of the layer is d_g. 2DEG sheet electron density Σ depends on the gate bias voltage $V(t)$. In our basic equivalent circuit model we will neglect nonlinear effects and consider its gate voltage

dependence in the form:

$$\Sigma = \Sigma_0 + \frac{\varepsilon_0 \varepsilon V_g}{e d_g} = \Sigma_0 (1 - \frac{V_g}{V_{th}}), \tag{2}$$

where Σ_0 is electron sheet concentration at $V_g = 0$, and V_{th} is the threshold voltage. As it follows from Eqs. (1) and (2), resonant frequencies of plasma oscillations in the 2DEG channel depend on the gate length and can be tuned by the gate bias voltage.
To express the components of electrical equivalent circuit in terms of physical parameters of the 2DEG system one may invert the Drude formula for the frequency dependent conductivity of the 2DEG and obtain its complex resistivity $\rho(\omega)$:

$$\rho(\omega) = \frac{m^*}{\Sigma e^2 \tau_{tr}} (1 + i\omega\tau_{tr}). \tag{3}$$

where $\tau_{tr} = \frac{m^*}{e}\mu$ is the transport or momentum scattering time and μ is electron mobility in the channel. The 2DEG complex resistivity contains purely resistive as well as inductive components (first and second terms in the right-hand side of Eq. (3), respectively). Therefore, to provide correct equivalent circuit representation of the system in question one should include not only the resistance of the 2DEG channel but inevitably its kinetic inductance (Burke,2000) associated with the inertia of the electrons in it. Furthermore, both resistance and inductance will depend on the gate bias voltage. For proper description of the system this fact should be also accounted for. Due to similarity of electromagnetic wave propagation in the gated 2DEG channel to that in a transmission line the distributed RC-circuit topology has been proposed for modeling of high-frequency effects in the gated 2DEG (Yeager, 1986). Later kinetic inductance has been added (Burke,2000) to distributed RC-circuit model modifying it into $R\mathcal{L}C$ distributed circuit model which we will use.
Combining Eqs. (2) and (3), for the distributed resistance R_g and kinetic inductance $\mathcal{L}_g$ of the gated portion of 2DEG channel we obtain the following expressions:

$$R_g = \frac{1}{e\mu\, W\Sigma_0(1 - \frac{V_g}{V_{th}})} = \frac{R_0}{1 - \frac{V_g}{V_{th}}}, \tag{4}$$

$$\mathcal{L}_g = \frac{m^*}{e^2 W\, \Sigma_0(1 - \frac{V_g}{V_{th}})} = \frac{\mathcal{L}_0}{1 - \frac{V_g}{V_{th}}}, \tag{5}$$

where W is the width of the device, R_0 and $\mathcal{L}_0$ are 2DEG channel resistance and inductance per unit length at $V_g = 0$. A distinctive feature of our equivalent circuit model is that it takes into account the dependence of the resistance R_g and inductance $\mathcal{L}_g$ on the gate bias voltage V_g (Khmyrova,2007). In this section the gate contact-2DEG channel system is considered as an ideal, i.e., fringing effects are neglected. Under this assumption its distributed capacitance can be expressed in the standard form:

$$C_g = \frac{\varepsilon_0 \varepsilon W}{d_g}, \tag{6}$$

To account for the losses due to, for example, leakage through the dielectric under the gate contact, relevant conductance G_l should be added in parallel with capacitance C_g.

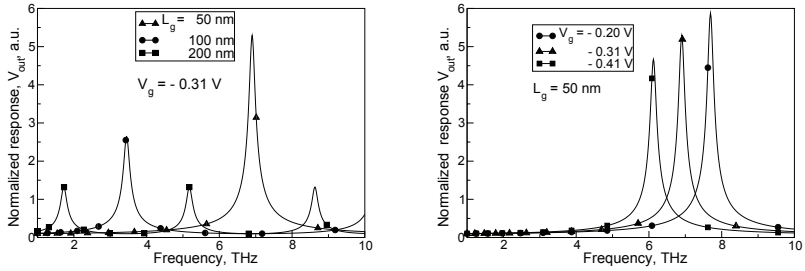

(a) (b)

Fig. 2. Normalized frequency response of the HEMT at (a) different gate lengths and $V_g = -0.31$ V; and (b) different gate bias voltages and $L_g = 50$ nm.

2.2 Results of IsSpice simulation

The developed distributed equivalent circuit of the gated 2DEG channel with $R\mathcal{L}C$-components described by Eqs. (4)-(6) is shown in Fig. 1b. It was used to simulate frequency performance of the InAlAs/InGaAs HEMT with IsSpice software which is the version of SPICE developed by Intusoft. In the simulation experiment the gated part of the 2DEG channel has been represented by a lossy transmission line component, chosen from IsSpice component library. R_g, $\mathcal{L}_g$ and C_g of the TL were calculated using Eqs. (4)-(6) and device geometrical and physical parameters listed in Table 1. First, we neglect leakage losses setting $G_l = 0$ and consider "open circuit" configuration, i.e., assume that part of the device adjacent to its gated 2DEG portion has very high resistance.

Normalized frequency response V_{out} simulated at different gate lengths L_g and $V_g = -0.31$ V is shown in Fig. 2a. Fig. 2a reveals pronounced resonant behavior with resonant peaks at frequencies corresponding to those determined by Eq. (1). The increase of the gate length L_g results in the fundamental resonant frequency reduction in line with Eq. (1). The decrease of the gate bias voltage V_g at a fixed gate length results in a decrease of the electron concentration beneath the gate contact which, in turn, leads to a resonant frequency reduction as it is shown in Fig. 2b. In other words, Fig. 2b illustrates the possibility to tune the frequency of plasma oscillations by the gate bias voltage.

Simulation using equivalent circuit approach makes it possible to evaluate quickly the influence of such factors as leakage through the dielectric separating the gate contact and 2DEG channel on the HEMT performance in the regime of excitation of plasma oscillations. Fig. 3 demonstrates the damping of oscillatory behavior of the response caused by the leakage through the dielectric separating the gate contact and 2DEG. When the conductivity across this layer increases, say, from $G_l/G_g = 0$ to $G_l/G_g = 2$ (as in Fig. 3) amplitude of plasma oscillations in the HEMT 2DEG channel decreases.

In real HEMT structures ungated regions are rather large, usually their length $L_c >> L_g$. It was assumed that such ungated regions can influence plasma oscillations excited in the 2DEG channel (Satou,2003) as well as parasitic stray capacitance and load resistors. To complete the basic equivalent circuit model we include also lumped resistance and inductance of the

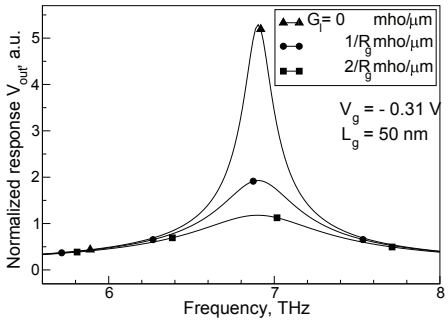

Fig. 3. Normalized HEMT frequency response at different leakage conductance G_l, $L_g = 50$ nm and $V_g = -0.31$ V.

ungated region of the 2DEG channel with the length L_c

$$R_c = R_0\, L_c, \qquad \mathcal{L}_c = \mathcal{L}_0\, L_c. \tag{7}$$

To account for parasitic capacitance a capacitor C_s has been added in parallel with resistance R_c and inductance $\mathcal{L}_c$.

Gate length	L_g	nm	50
Gate width	W	μ m	50
Thickness of the layer under the gate	d	nm	17
Length of ungated region	L_{un}	nm	100
Sheet electron density	Σ_d	cm^{-2}	5×10^{12}
Electron mobility	μ	$cm^2\ V^{-1}\ s^{-1}$	4×10^4
Threshold voltage	V_{th}	V	- 0.764
Dielectric constant	ε		12.7

Table 1. Structure parameters

2.3 Transmission line load termination concept and reflection coefficient at the gated/ungated 2DEG channel interface

Exploiting further the similarity to a transmission line, one may treat the part of the device including the ungated portion of the 2DEG channel, contacts, etc., (see Fig. 1b) as a "load" with the impedance

$$Z_L = \frac{R_c + j\omega\mathcal{L}_c}{j\omega C_s(R_c + j\omega\mathcal{L}_c + \frac{1}{j\omega C_s})} \tag{8}$$

According to the concept of a transmission line (Collin,2007) at its "load" termination reflection coefficient (the ratio of reflected and incident waves) is given by the following formula:

$\Gamma = \dfrac{Z_L - Z_g}{Z_L + Z_g}$, where $Z_g = \sqrt{\dfrac{R_g + j\omega\mathcal{L}_g}{j\omega C_g}}$ is the transmission line characteristic impedance in the absence of leakage losses $G_l = 0$. In the frequency range of interest and given structural parameters one may assume $R_g/\omega\mathcal{L}_g << 1$ and simplify characteristic impedance as

$$Z_g \simeq \sqrt{\frac{\mathcal{L}_g}{C_g}}\sqrt{1 - j\frac{R_g}{\omega\mathcal{L}_g}} \tag{9}$$

The modulus and phase of reflection coefficient Γ are shown in Figs. 4a and 4b, respectively, at different lengths of contact region L_c. At given structural parameters modulus of reflection coefficient does not approach zero, or, in other words, the "load" impedance is mismatched. In regular transmission lines any reflection at the load termination is undesirable and efforts are usually being made to eliminate it. On the contrary, for the excitation and build up of plasma waves in the system under discussion the "load" impedance mismatch seems to be beneficial.

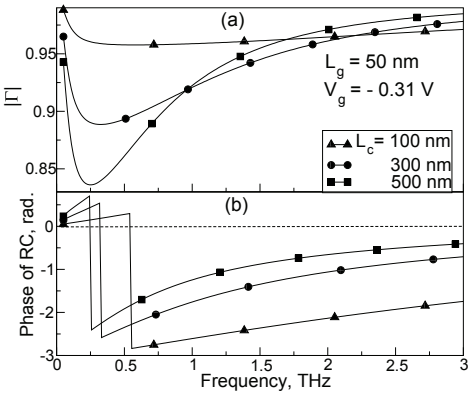

Fig. 4. Modulus (a) and phase (b) of the reflection coefficient at the load termination of the distributed circuit corresponding to the interface between gated and ungated parts of the 2DEG channel.

It was demonstrated with IsSpice simulation that the increasing length of ungated region causes the transformation of resonant peaks and shift of plasma resonances (Khmyrova,2007) although the effect was smaller comparing to that predicted by the model developed in (Satou,2003). Indeed, the situation in real devices is much more complicated. In particular, cap layer incorporated in the device structure to reduce an access source/drain contacts resistance may affect its frequency performance.

3. Impact of fringing effects on resonant frequencies of plasma oscillations

Another factor reducing the resonant plasma frequencies can be related to the nonideality of the gate contact–2DEG capacitance, i.e., fringing effects (Suemitsu,1998; Nishimura,2009). As it follows from Eq. (1) scaling down of the gate length L_g should result in the increase of the fundamental resonant plasma frequency. It seems quite natural that the gate length reduction

should be accompanied by the relevant reduction of the thickness of the layer separating the gate contact and 2DEG surface. However, there are technological restrictions on the possible reduction of the thickness d_g. As a result, fringing of the electric field created by gate bias voltage may become sufficiently strong and its contribution should not be neglected.

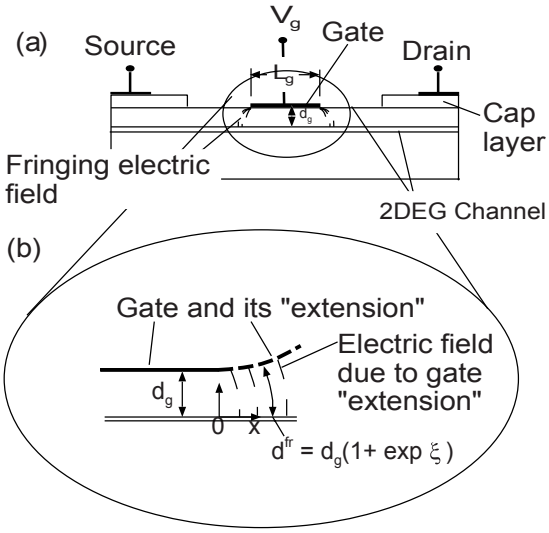

Fig. 5. Schematic of the HEMT structure (a) and model of "extended" gate (b).

3.1 Analytical model

We assume that width W of the HEMT-like structure schematically shown in Fig. 5a is large enough to provide the uniformity in the direction perpendicular to the page so that we can focus on the variation of the electric field and other related values only along x-axis indicated in Fig. 5b. Reference point $x = 0$ coincides with the edge of the gate contact, so that points with $-L_g < x < 0$ correspond to the 2DEG channel beneath the gate contact and $x > 0$ - to the ungated 2DEG channel region subjected to the fringing electric field. The thickness of the 2DEG channel is assumed to be negligibly small.

The distribution of fringing electric field at the 2DEG channel surface is similar to that in the middle plane of the fringed parallel plate capacitor with plate length L_g and separation $2d_g$. Using the conformal mapping approach elaborated in Ref. (Morse,1953) we can express in parametric form the fringing electric field distribution

$$E(\xi) = \frac{V_g}{d_g} \frac{1}{1 + \exp \xi}, \tag{10}$$

and x-coordinate

$$x = \frac{d_g}{\pi L_g}(1 + \xi + \exp \xi), \tag{11}$$

where ξ is a parameter and V_g is the gate bias voltage.

It is worth to note that electric field distribution in the structure with the gate contact extended in the direction $x > 0$ in such a way that separation between the gate contact and 2DEG surface varies as $d^{fr} = d_g(1 + \exp\xi)$ (see Fig. 5(b)) will be also described by Eq. (10) and be similar to fringing field. Furthermore, the ungated part of 2DEG channel subjected to the fringing electric field can be treated in the same way as its gated portion. For the 2DEG sheet electron density in the ungated fringed region one can write down an expression similar to Eq. (2):

$$\Sigma_{fr} = \Sigma_0^{fr} + \frac{\varepsilon\varepsilon_0 V_g}{e d_g(1 + \exp\xi)}. \tag{12}$$

Here Σ_0^{fr} is sheet electron density in the fringed region at $V_g = 0$. The threshold voltage in the fringed region can be expressed as

$$V_{th}^{fr}(\xi) = -\frac{e\Sigma_0^{fr} d_g(1 + \exp\xi)}{\varepsilon\varepsilon_0} = \frac{\Sigma_0^{fr}}{\Sigma_0} V_{th}^0 (1 + \exp\xi), \tag{13}$$

where Σ_0 and V_{th}^0 are the surface charge density at $V_g = 0$ and threshold voltage for the 2DEG channel beneath the gate contact. On the other hand, threshold voltage is determined by physical and structural parameters (Delagebeaudeuf,1982): $V_{th} = \phi_M - \Delta E_c - V_p$, where ϕ_M is Schottky barrier height due to metalization of the gate contact, ΔE_c is conduction band discontinuity at the InAlAs-InGaAs heterointerface, and $V_p = e\Sigma_d\, d_d/\varepsilon\varepsilon_0$ for δ-doped HEMT (Mahajan,1998) where Σ_d and d_d are the dopant concentration and distance between the δ-doping plane and metal contact. In the fringed region the latter term is also position dependent and can be presented as $V_p^{fr}(\xi) = V_p^0(1 + \exp\xi)$ resulting in the threshold voltage described by the following expression:

$$V_{th}^{fr}(\xi) = \phi_M - \Delta E_c - V_p^0(1 + \exp\xi) = V_{th}^0 - V_p^0 \exp\xi, \tag{14}$$

which implies that to deplete 2DEG in the fringed region higher bias voltage should be applied to the gate contact. One can express Σ_0^{fr} from Eqs. (14) and (15), substitute it into Eq. (13) and arrive at

$$\Sigma_{fr} = \frac{\Sigma_0}{1 + \exp\xi}\left(1 - \frac{V_g}{V_{th}^0}\right)\left(1 - \frac{V_p^0 \exp\xi}{V_{th}^0 - V_g}\right). \tag{15}$$

Fig. 6 shows spatial distribution of the sheet electron density Σ_{fr} for different ratios d_g/L_g at gate voltage $V_g = -0.1$ V, $\phi_M = 0.62$ V, $\Delta E_c = 0.53$ eV (Mahajan,1998), $\Sigma_d = 5 \times 10^{12}$ cm^{-2} and $d_d = 12$ nm (El Fatimy,2006).

It is seen from Fig. 6, that at small ratios $d_g/L_g << 1$ sheet electron density near the gate contact edge varies sharply, i.e., fringing of the electric field is small and can be neglected.

Scaling down the gate length and gate-to-channel separation to $L_g = 50$ nm and $d_g = 17$ nm results in the ratio $d_g/L_g \simeq 0.34 < 1$. As one can see from Fig. 6 , at this ratio the fringing electric field extends at a distance L_{fr} up to several L_g. The ungated regions of length $L_c \leq L_{fr}$ being affected by the fringing field are no longer different from the gated region of the 2DEG channel and should be treated in the same way.

Thus, fringing electric field causes the extension of the 2DEG channel region controlled by the gate bias voltage V_g beyond the area covered by the gate contact. Moreover, as it is seen from Fig. 6, the fringing of the electric field influences the sheet electron density not only in the ungated regions on both sides of the gate contact, but also beneath the contact itself.

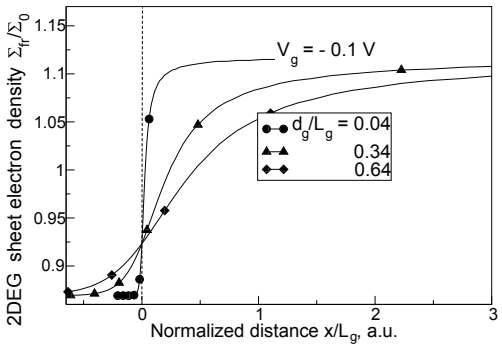

Fig. 6. 2DEG sheet electron density distribution along HEMT channel in the presence of fringing electric field at different ratios of d_g/L_g. Reference point $x = 0$ corresponds to the gate contact edge.

Due to symmetry of the HEMT structure one may consider only its half, i.e., $-0.5L_g \leq x \leq L_{fr}$ when calculating the phase change θ_{fr} of the wave traveling along the gated and fringed ungated regions (Andress,2005) of the 2DEG channel a distance $L_g + 2L_{fr}$

$$\theta_{fr} = 2\omega^{fr} \int_{x=-0.5}^{L_{fr}} \frac{dx}{s_{fr}}, \tag{16}$$

where wave's phase velocity can be expressed using Eq. (15) in the form

$$s_{fr} = \sqrt{\frac{e}{m^*}(V_g - V_{th}^0)(1 + \frac{V_p^0}{V_g - V_{th}^0} \exp\xi)} \tag{17}$$

Substitution of Eq. (17) into Eq. (16) is accompanied by the change of the variables of integration from x to ξ. For the upper limit of integration ξ_2 from Eq. (2) $L_{fr} = \frac{d_g}{\pi}(1 + \xi_2 + \exp\xi_2)$ we find $\exp(\xi_2) \simeq \frac{\pi L_{fr}}{2d_g}$. For the lower integral limit we have an equation $-0.5L_g = \frac{d_g}{\pi}(1 + \xi_1 + \exp\xi_1)$, where $\xi_1 < 0$. Substituting the modulus $|\xi_1|$ in the latter condition we get: $|\xi_1| \simeq 1 + \frac{\pi L_g}{2d_g}$. After integration from the condition for standing wave existence (Dyakonov,1996) we finally obtain the fundamental plasma resonant frequency in the presence of fringing effects

$$f^{fr} \approx \frac{f_0}{1 + \frac{4d_g}{L_g \pi R_v}\left(\sqrt{1 + \frac{\pi R_v L_{fr}}{2d_g}} - 1\right) + \chi}, \tag{18}$$

where f_0 is the fundamental frequency of plasma oscillations in the ideal case when no fringing occurs (from Eq. (1) $f_0 = \Omega/2\pi$),

$$\chi = \frac{2d_g}{\pi L_g}\left(1 + \ln\frac{4}{R_v} - 2\sqrt{\frac{2d_g}{\pi R_v L_{fr}}}\right), \tag{19}$$

and $R_v = V_p^0/(V_g - V_{th}^0)$.

3.2 Cascaded transmission line model and results of IsSpice simulation

The spanning of the 2DEG channel region controlled by the gate bias voltage beyond the area covered by the gate contact caused by fringing of the electric field requires appropriate modification of the equivalent circuit model previously developed. To represent the fringed ungated region with nonuniform sheet electron density distribution and position dependent distance d^{fr} between the "extended" gate and 2DEG channel as an equivalent electric circuit we partitioned it into small segments (Andress,2005). In each such segment sheet electron density is supposed to be uniform and distance d^{fr} constant so that they can be represented by a uniform transmission lines $TL_{1,2,...,N}$. The cascaded TL model for the gated and ungated fringed 2DEG channel regions is schematically shown in Fig. 7. Relevant $R_{fr}, \mathcal{L}_{fr}, C_{fr}$ components are derived using Eq. (15) in the form

$$R_{fr} = R_g \frac{1+\exp\xi}{1+\frac{V_p^0}{V_g - V_{th}^0}\exp\xi},$$

$$\mathcal{L}_{fr} = \mathcal{L}_g \frac{1+\exp\xi}{1+\frac{V_p^0}{V_g - V_{th}^0}\exp\xi}, \qquad C_{fr} = \frac{C_g}{1+\exp\xi}, \tag{20}$$

whereR_g, $\mathcal{L}_g$ and C_g are determined by Eqs. (4)-(6).
In the developed cascaded equivalent circuit the ungated fringed region has been represented by 10 uniform TLs. In the IsSpice simulation TL input voltage corresponded to the gate bias voltage which contained dc and ac components. ac analysis has been conducted and response has been measured in the open circuit configuration. Test simulations performed for 5-, 10- and 15-sections model of the ungated fringed region revealed very close fundamental resonant plasma frequencies for 10 and 15 sections. Simulated frequency response of the HEMT is shown in Fig. 8. It is clearly seen from the simulation results of Fig. 8 that fringing effects cause the reduction of the resonant frequency of plasma oscillations.

4. Comparison of Theoretical and Experimental Data

Fig. 9 shows dependences of fundamental resonant plasma frequency versus gate bias voltage V_g calculated for the InAlAs/InGaAs HEMT with the gate length $L_g = 50$ nm, and structure parameters taken from Ref.(El Fatimy,2006). Curve (1) calculated using Eq. (1) corresponds to the ideal case. Curve (2) represents experimental data extracted from Ref.(El Fatimy,2006). Curve (3) has been calculated using model of Ref.(Satou,2003) which takes into account ungated regions. Curves (4) and (5) were calculated and simulated using fringing effect model. Plasma frequencies of curve 4 were calculated using Eq. (17) under the assumption based on Fig. 6 that for the ratio $d_g/L_g = 0.34$ the fringing field spreads over the whole ungated regions of length $L_c = 2 \times L_g$ on both sides of the gate contact, i.e., $L_{fr} = 2 \times 100 = 200$ nm.

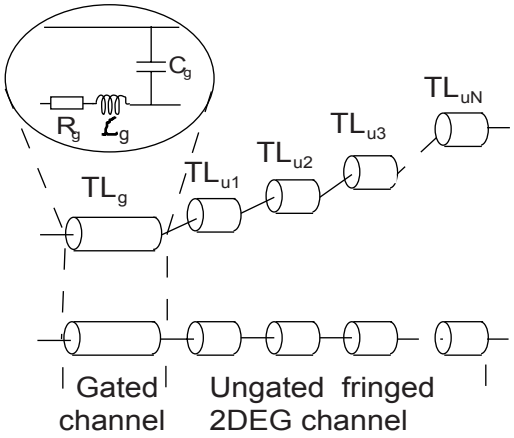

Fig. 7. Cascaded TL model for the HEMT in the presence of fringing effects. Gated 2DEG channel is represented by a single uniform TL. Ungated fringed 2DEG channel region is partitioned so that each part can be represented by uniform TL (TL_{u1}, TL_{u2},... TL_{uN}).

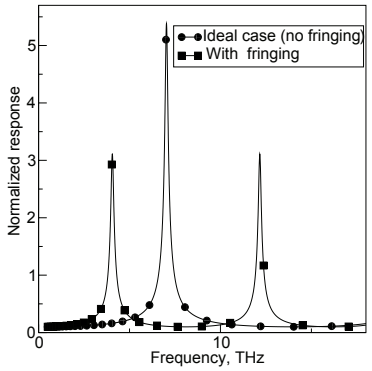

Fig. 8. Frequency response of the HEMT simulated with IsSpice software for the ideal case when fringing effects are neglected (uniform TL model for the gated channel) and for the case when ungated 2DEG channel region is fringed (cascaded TL model for the gated and fringed ungated HEMT channel regions).

As it was mentioned previously experimentally observed plasma resonant frequencies (curve 2) were much lower comparing to those predicted by Eq. (1). The model which takes into account the contribution of ungated regions (curve 3)shows, at a first glance, practically ideal agreement with experimental data. However, the incorporation of the possible contribution of some other factors, for example, cap layer may result in deviation from such ideal agreement. On the other hand, comparing curves 4 and 5 with experimental data of curve

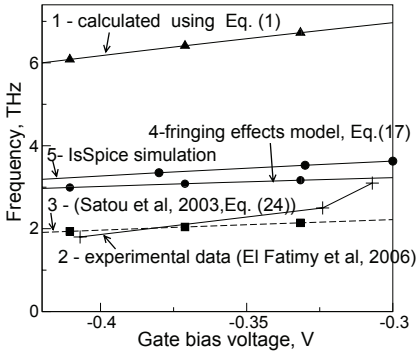

Fig. 9. Fundamental frequency of plasma oscillations: 1– Ideal case, calculated using Eq. (1); 2 – Experimental data extracted from Ref. (El Fatimy, 2006); 3 – Model for impact of ungated regions, Eq. (24) of Ref. (Satou,2003); 4 – model accounting for fringing effects, Eq. (17); 5 – Results of IsSpice simulation.

2 one can say about reasonably good agreement between them keeping in mind that further reduction of plasma frequencies is possible due to contribution of other factors, in particular, cap layer.

5. Chapter summary

In conclusion, we develop simple distributed circuit model of the HEMT-like structure to study the effects associated with the excitation of plasma oscillations in its 2DEG channel. The circuit components of the model are related to physical and geometrical parameters of the structure. Moreover, the dependence of the resistance and kinetic inductance of the gated 2DEG channel portion on gate bias voltage has been taken into account. The developed electric equivalent circuit has been used to simulate HEMT frequency performance with IsSpice software. Model accounting for the fringing effects contribution to the plasma frequency reduction is proposed. Using the concept of "extended" gate the sheet electron density distribution in the fringed ungated region of the 2DEG channel is estimated and the expression for the resonant plasma frequency in the presence of fringing effects is derived. The basic distributed circuit model has been modified into cascaded TL line model to account for the impact of fringing effects on the resonant plasma frequencies. Simulated HEMT frequency response shows the decrease of resonant frequency related to the fringing effects. The results of our model are in rather good agreement with experimental data admitting also further possible frequency reduction due to other factors, for example, the cap layer.

6. References

[1] Allen, S. J.; Tsui, D. C.; & Logan, R.A. (1977) Observation of the two-dimensional plasmon in silicon inversion layers. *Phys. Rev. Lett*, Vol. 38, 980-983.

[2] Andress, W. F. and Ham, D. (2005) Standing wave oscillators utilizing wave-adaptive tapered transmission lines, *IEEE J. Solid State Circuits*, Vol. 40, pp. 638-651.
[3] Burke, P. J.; Spielman, I. B.; Eisenstein, J. P.; Pfeiffer, L. N.; & West, K. W. (2000) High frequency conductivity of the high-mobility two-dimensional electron gas, *Appl. Phys. Lett.* Vol. 76, 745-747.
[4] Chaplik, A V. (1972) Possible crystallization of charge carriers in low-density inversion layers. *Sov. Phys. JETP*, Vol. 35, 395–398.
[5] Collin, R. E. (1992) *Foundations for Microwave Engineering* (McGrow-Hill, Inc., New York, 1992)
[6] Delagebeaudeuf, D. & Linh, N. T. (1982) Metal-(n) AlGaAs-GaAs two-dimensional electron gas FET, *IEEE Trans. Electron Devices*, Vol. ED-29, 955–960.
[7] Dyakonov, M. & Shur, M. (1993) Shallow water analogy for a ballistic field effect transistor: New mechanism of plasma wave generation by dc current *Phys. Rev. Lett.,* Vol. 71, 2465-2468.
[8] Dyakonov, M. & Shur, M. (1996) Plasma wave electronics: novel terahertz devices using two dimensional electron fluid, *IEEE Trans. Electron Device*, vol. 43, 1640-1645, 1996.
[9] El Fatimy, A.; Teppe, F.; Dyakonova, N.; Knap, W.; Seliuta, D.; Valusis, G.; Shchepetov, A.; Roelens, Y.; Bollaert, S.; Cappy, A.; & Rumyantsev, S. (2006). Resonant and voltage-tunable terahertz detection in InGaAs/InP nanometer transistors, *Appl. Phys. Lett.*, Vol. 89, 131926.
[10] Khmyrova, I. & Seijyou, Yu. (2007) Analysis of plasma oscillations in high-electron mobility transistor-like structures: Distributed circuit approach, *Appl. Phys. Lett.,* Vol. 91, 143515.
[11] Knap, W.; Kachorovskii, V.; Deng, Y.; Rumyantsev, S.; Lu, J.Q.; Gaska, R.; Shur, M.S.; Simin, G.; Hu, X.; Asif Khan, M.; Sailor, C.A.; & Brunel, L.C. (2002) Nonresonant detection of terahertz radiation in field effect transistors *J. Appl. Phys.* Vol. 91, 9346–9353.
[12] Lu,J.; Shur,M.S.; Hesler,J.L.; Sun, L.; & Weikle, R. (1998) Terahertz detector utilizing two-dimensional electronic fluid, *IEEE Electron Device Lett.*, Vol. 19, 373-375.
[13] Mahajan,A.; Arafa, M.; Fay, P.; Caneau, C.; & Adesida, I. (1998). Enhancement-mode high electron mobility transistors (E-HEMT's) lattice-matched to InP, *IEEE Trans. Electron Devices*, Vol. ED-45, 2422-2429.
[14] Morse, Ph. M. & Feshbach, H. (1953) *Methods of Theoretical Physics* (McGrow-Hill, Inc., New York, 1953)
[15] Nishimura,T.; Magome, N.; Khmyrova, I.; Suemitsu, T.; Knap, W.; & Otsuji, T. (2009). Analysis of fringing effect on resonant plasma frequency in plasma wave devices, *Jpn. J. Appl. Phys.*, Vol. 48, 04C096.
[16] Otsuji, T.; Hanabe, M.; & Ogawara, O. (2004). Terahertz plasma wave resonance of two-dimensional electrons in InGaP/InGaAs/GaAs high-electron-mobility transistors, *Appl. Phys. Lett.*, vol. 85, 2119.
[17] Satou, A.; Khmyrova, I.; Ryzhii, V.; & Shur, M. (2003) Plasma and transit-time mechanisms of the terahertz radiation detection in high-electron-mobility transistors. *Semicond. Sci. Technol.* Vol. 18, 460 .
[18] Satou, A.; Ryzhii, V.; Khmyrova, I.; Ryzhii, M.; & Shur, M. (2004) Characteristics of a terahertz photomixer based on a high-electron mobility transistor structure with optical input through the ungated regions. *J. Appl. Phys.* Vol. 95, 2084–2089.
[19] Shur, M. S. & Ryzhii, V. (2003) Plasma wave electronics. *Int. J. High. Speed Electron Syst.* Vol. 13, 575-600.

[20] Suemitsu, T.; Enoki, T.; Yokoyama, H.; & Ishii, Y. (1998) Improved recessed-gate structure for sub-01-μm-gate InP-based high electron mobility transistors, *Jpn. J. Appl. Phys.*, Vol. 37, pp. 1365-1372.

[21] Teppe, F.; Knap, W.; Veksler, D.; Shur, M. S.; Dmitriev, A. P.; Kacharovskii, V. Yu.; & Rumyantsev, S. (2005). Room-temperature plasma waves resonant detection of sub-terahertz radiation by nanometer field-effect transistor, *Appl. Phys. Lett.*, Vol. 87, 052107.

[22] Tsui, D.C.; Gornik, E. & Logan, R.A. (1980) Far infrared emission from plasma oscillations of Si inversion layers, *Solid State Commun.*, Vol. 35, 875-877.

[23] Veksler,D.; Teppe, F.; Dmitriev, A. P.; Kacharovskii, V. Yu.; Knap, W.; & Shur, M. S. Detection of terahertz radiation in gated two-dimensional structures governed by dc current. *Phys. Rev.* Vol. B 73 125328.

[24] Weikle, R.; Lu, J.; Shur, M.S.; (2006) & Dyakonov, M. (1996) Detection of microwave radiation by electronic fluid in high electron mobility transistors, *Electron. Lett.*, vol. 32, 2148-2149.

[25] Yeager, H. R. & Dutton, R. W. (1986) Circuit simulation models for the high electron mobility transistor, *IEEE Trans. Electron Devices*, Vol. ED-33, pp. 682–692.

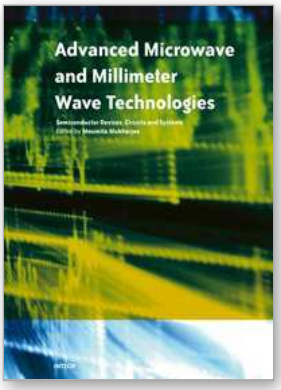

Advanced Microwave and Millimeter Wave Technologies
Semiconductor Devices Circuits and Systems
Edited by Moumita Mukherjee

ISBN 978-953-307-031-5
Hard cover, 642 pages
Publisher InTech
Published online 01, March, 2010
Published in print edition March, 2010

This book is planned to publish with an objective to provide a state-of-the-art reference book in the areas of advanced microwave, MM-Wave and THz devices, antennas and systemtechnologies for microwave communication engineers, Scientists and post-graduate students of electrical and electronics engineering, applied physicists. This reference book is a collection of 30 Chapters characterized in 3 parts: Advanced Microwave and MM-wave devices, integrated microwave and MM-wave circuits and Antennas and advanced microwave computer techniques, focusing on simulation, theories and applications. This book provides a comprehensive overview of the components and devices used in microwave and MM-Wave circuits, including microwave transmission lines, resonators, filters, ferrite devices, solid state devices, transistor oscillators and amplifiers, directional couplers, microstripeline components, microwave detectors, mixers, converters and harmonic generators, and microwave solid-state switches, phase shifters and attenuators. Several applications area also discusses here, like consumer, industrial, biomedical, and chemical applications of microwave technology. It also covers microwave instrumentation and measurement, thermodynamics, and applications in navigation and radio communication.

How to reference
In order to correctly reference this scholarly work, feel free to copy and paste the following:

Irina Khmyrova (2010). Study of Plasma Effects in HEMT-like Structures for THz Applications by Equivalent Circuit Approach, Advanced Microwave and Millimeter Wave Technologies Semiconductor Devices Circuits and Systems, Moumita Mukherjee (Ed.), ISBN: 978-953-307-031-5, InTech, Available from: http://www.intechopen.com/books/advanced-microwave-and-millimeter-wave-technologies-semiconductor-devices-circuits-and-systems/study-of-plasma-effects-in-hemt-like-structures-for-thz-applications-by-equivalent-circuit-approach

INTECH
open science | open minds

InTech Europe
University Campus STeP Ri
Slavka Krautzeka 83/A
51000 Rijeka, Croatia
Phone: +385 (51) 770 447
Fax: +385 (51) 686 166

InTech China
Unit 405, Office Block, Hotel Equatorial Shanghai
No.65, Yan An Road (West), Shanghai, 200040, China
中国上海市延安西路65号上海国际贵都大饭店办公楼405单元
Phone: +86-21-62489820
Fax: +86-21-62489821